

Electron Scattering in Perovskite-Oxide Ferroelectric Semiconductors

S. H. WEMPLE, M. DiDOMENICO, JR., AND A. JAYARAMAN

Bell Telephone Laboratories, Murray Hill, New Jersey 07974

(Received 21 October 1968; revised manuscript received 30 December 1968)

This paper reports new data on the hydrostatic-pressure dependence of the conductivity and static dielectric constant, as well as new Hall-effect data taken over a wide temperature range, in the perovskite-oxide ferroelectrics KTaO_3 , SrTiO_3 , BaTiO_3 , and $\text{KTa}_{1-x}\text{Nb}_x\text{O}_3$ ($x=0.02, 0.1, \text{ and } 0.35$). From the linear dependence of the electron mobility μ and the reciprocal dielectric constant $1/\epsilon$ on pressure in all materials studied, we conclude that $\mu \propto 1/\epsilon + \text{const}$. Based on the observed temperature dependence of the Hall mobility and the Curie-Weiss behavior of ϵ , we conclude further that in the perovskite oxides the temperature dependence of the mobility is given by the empirical expression $\mu \propto T^{-3.5}(T - T_0 + T^*)$, $T > T_0$, where T^* is an experimental constant and T_0 is the Curie-Weiss temperature ($T_0=4^\circ\text{K}$ and $T^*\approx 140^\circ\text{K}$ for KTaO_3 , $T_0=32^\circ\text{K}$ and $T^*\approx 77^\circ\text{K}$ for SrTiO_3 , $T_0=287^\circ\text{K}$ and $T^*\approx 70^\circ\text{K}$ for $\text{KTa}_{0.65}\text{Nb}_{0.35}\text{O}_3$, and $T_0=395^\circ\text{K}$ and $T^*\approx 85^\circ\text{K}$ for BaTiO_3). Our experimental results are shown to be inconsistent with previously reported suggestions that the electron mobility in the perovskite oxides is dominated by LO-mode scattering. We suggest, instead, that the electron mobility is determined by a new and strong electron-phonon interaction involving critical-point lattice-polarization fluctuations associated with the soft TO mode.

I. INTRODUCTION

ALTHOUGH much is known about the transport properties of the ferroelectric perovskite oxides (e.g., SrTiO_3 , KTaO_3 , BaTiO_3), there is at present no satisfactory description of the dominant electron-phonon interaction. It has been suggested that the strongly polar nature of these materials should lead to electron scattering dominated by the longitudinal optical (LO) phonons. Recently, Frederikse and Hosler¹ compared their mobility temperature-dependence data in SrTiO_3 to the Low-Pines² intermediate coupling polaron theory and concluded that LO phonons are the major source of electron scattering in this material. This conclusion differs from that previously drawn by the present authors³ based on the hydrostatic-pressure dependence of the conductivity and static dielectric constant in several perovskite oxides (including SrTiO_3). By extending our hydrostatic-pressure and Hall-effect measurements to cover a wider temperature range and a larger group of materials than previously reported we have attempted to delineate more clearly the electron scattering mechanism in these materials. The results of our present investigation⁴ confirm our earlier proposal and illustrate the difficulty associated with attempts to unequivocally determine electron scattering mechanisms from mobility temperature dependence data alone.

Previously^{3,4} we proposed the following empirical relationship between electron mobility μ and the static dielectric constant ϵ based on similarities in their hydrostatic-pressure dependences:

$$\mu = f(T)(1/\epsilon + \text{const}), \quad (1)$$

¹ H. P. R. Frederikse and W. R. Hosler, *Phys. Rev.* **161**, 822 (1967).

² F. E. Low and D. Pines, *Phys. Rev.* **98**, 414 (1955).

³ S. H. Wemple, A. Jayaraman, and M. DiDomenico, Jr., *Phys. Rev. Letters* **17**, 142 (1966).

⁴ For a preliminary account of this work, see M. DiDomenico, Jr., S. H. Wemple, and A. Jayaraman, in *Proceedings of the Ninth International Conference on the Physics of Semiconductors* (to be published).

where $f(T)$ is a temperature-dependent factor. Because ϵ is intimately related to the frequency ω_{TO} of the soft ferroelectric transverse optic (TO) lattice mode, we suggested that the soft TO mode is the primary source of electron scattering in the perovskite oxides, but did not describe the nature of the interaction in detail. In this paper we present further experimental evidence for the validity of Eq. (1), and we also propose a model describing scattering in terms of random conduction-band perturbations produced by lattice-polarization (critical-point) fluctuations.⁴

II. EXPERIMENTAL PROCEDURE AND RESULTS

In an earlier publication³ we proposed that Eq. (1) is valid at room temperature in KTaO_3 , SrTiO_3 , and $\text{KTa}_{0.65}\text{Nb}_{0.35}\text{O}_3$, based on the hydrostatic-pressure dependences of electrical conductivity and reciprocal static dielectric constant. We have since extended these measurements⁴ to other materials and temperatures in an effort to establish the general validity of Eq. (1). The hydrostatic-pressure experiments were performed using a piston cylinder device described elsewhere.⁵ The pressure-transmitting fluid, a 50/50 mixture of *n*-pentane and isoamyl alcohol, was contained in a Teflon cell. Hydrostatic pressures up to 35 kbar were readily achieved using this technique. For measurements at elevated temperatures (up to 140°C), the entire pressure plate was heated from the outside with heating tape. Pressure calibration was established using the Bi I-II transition at 25.4 kbar. For the four-terminal conductance measurements, van der Pauw sample shapes⁶ were used, and Ohmic contact to the four sample arms was made using vacuum-deposited titanium electrodes covered with an overlay of palladium. Fine leads were then soldered to the palladium. In order to facilitate making Ohmic contacts it proved advantageous to etch

⁵ A. Jayaraman, A. R. Hutson, J. H. McFee, A. S. Coriell, and R. G. Maines, *Rev. Sci. Instr.* **38**, 44 (1967).

⁶ L. J. van der Pauw, *Philips Res. Rept.* **13**, 1 (1958).

the crystal surfaces prior to deposition of the electrode materials. For most of the crystals, molten KOH contained in a silver crucible proved to be an effective etchant. In the case of BaTiO₃ a phosphoric acid solution was used as the etchant. Hydrostatic-pressure dependences of the reciprocal static dielectric constant were also obtained at temperatures between 22 and 140°C. For these measurements high-resistivity crystals were cut into thin plates and electroded with titanium palladium. The capacitance was measured as a function of pressure at 100 kHz using a Boonton capacitance bridge.

Figure 1 shows typical hydrostatic-pressure dependences of the electrical conductivity σ and reciprocal dielectric constant $1/\epsilon$ for three perovskite-oxide materials. Both σ and $1/\epsilon$ have been normalized to their zero-pressure values of σ^0 and $1/\epsilon^0$, respectively. In all crystals studied (i.e., SrTiO₃, BaTiO₃, KTaO₃, and KTa_{1-x}Nb_{2x}O₃), a linear relationship is observed between the hydrostatic pressure p and both σ and $1/\epsilon$. All of our hydrostatic-pressure results for four perovskite materials are summarized in Fig. 2, where we show the reciprocal pressure derivatives $[\partial(\sigma/\sigma^0)/\partial p]^{-1}$ and $[\partial(\epsilon^0/\epsilon)/\partial p]^{-1}$ as functions of temperature T . The straight lines in Fig. 2 are least-squares fits to the data. In the case of BaTiO₃, where data were obtained at only one temperature (140°C), the indicated straight lines are drawn parallel with a slope $(\partial/\partial T)[\partial(\epsilon^0/\epsilon)/\partial p]^{-1}$ given by Samara.⁷ We note immediately from Fig. 2 the following:

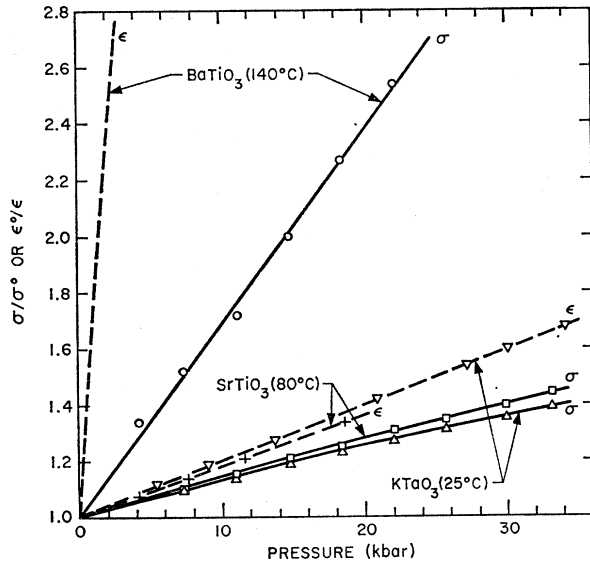


FIG. 1. Pressure dependence of the normalized conductivity σ/σ^0 and reciprocal dielectric constant ϵ^0/ϵ (σ^0 and ϵ^0 are zero-pressure values) in KTaO₃, SrTiO₃, and BaTiO₃. The temperatures indicated in parentheses refer to the temperature at which the data were taken. Above 20 kbar a small change in slope $\partial(\sigma/\sigma^0)/\partial p$ of unknown origin is observed for both KTaO₃ and SrTiO₃.

⁷ G. A. Samara, Phys. Rev. **151**, 378 (1966).

(i) There is a general trend of decreasing reciprocal slope with increasing ferroelectric Curie-Weiss temperature T_0 ($T_0=4^\circ\text{K}$ for KTaO₃, $T_0=32^\circ\text{K}$ for SrTiO₃, $T_0=287^\circ\text{K}$ for KTa_{0.65}Nb_{0.35}O₃, and $T_0=395^\circ\text{K}$ for BaTiO₃).

(ii) The temperature derivatives $(\partial/\partial T)[\partial(\sigma/\sigma^0)/\partial p]^{-1}$ and $(\partial/\partial T)[\partial(\epsilon^0/\epsilon)/\partial p]^{-1}$ are nearly the same in all four materials.

The pressure data shown in Figs. 1 and 2 can be understood if the conductivity and dielectric constant are related by the expression

$$\sigma \propto 1/\epsilon + \text{const.} \quad (2)$$

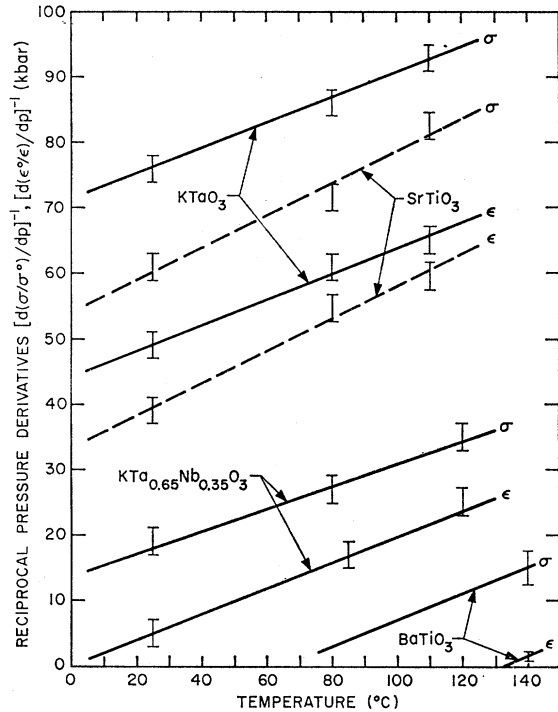


FIG. 2. Temperature dependence of the reciprocal pressure derivatives (reciprocal slopes in Fig. 1) in four perovskite ferroelectrics having Curie-Weiss temperatures T_0 ranging from 4 to 395°K, i.e., KTaO₃ ($T_0=4^\circ\text{K}$), SrTiO₃ ($T_0=32^\circ\text{K}$), KTa_{0.65}Nb_{0.35}O₃ ($T_0=287^\circ\text{K}$), and BaTiO₃ ($T_0=395^\circ\text{K}$).

Since ϵ obeys a Curie-Weiss law in the perovskite oxides, i.e.,

$$1/\epsilon = (T - T_0)/\epsilon_0 C, \quad (3)$$

where C is the pressure-independent Curie constant, and ϵ_0 is the free-space permittivity, we find that

$$[\partial(\epsilon^0/\epsilon)/\partial p]^{-1} = (T - T_0)(-\partial T_0/\partial p)^{-1}. \quad (4)$$

Substituting Eq. (3) into Eq. (2) and differentiating, we obtain

$$[\partial(\sigma/\sigma^0)/\partial p]^{-1} = (T - T_0 + T^*)(-\partial T_0/\partial p)^{-1}, \quad (5)$$

where T^* is a constant. The slopes of the straight lines in Fig. 2 for ϵ and σ data therefore give the rate of

decrease of the Curie-Weiss temperature T_0 with hydrostatic pressure, i.e., $-\partial T_0/\partial p$. In Table I we tabulate the quantity $-\partial T_0/\partial p$ obtained from both ϵ and σ data and find that these quantities are the same to within the experimental error. The values of T^* extracted from Fig. 2 using Eq. (5) are also listed in Table I. We note, finally, that Eqs. (4) and (5) predict the observed increase in reciprocal slopes with decreasing values of T_0 . The experimental hydrostatic-pressure results thus strongly support a relationship between electrical conductivity and reciprocal dielectric constant at a fixed temperature $T > T_0$ of the form given by Eq. (2). The temperature dependence of σ may therefore be expressed as

$$\sigma = g(T)(T - T_0 + T^*), \quad (6)$$

where $g(T)$ is a temperature factor determined below.

Further evidence in support of Eqs. (2) and (6) has been obtained from measurements of the conductivity temperature dependence at elevated pressures and from the temperature dependence of the electron Hall mobility. Hall-effect measurements were performed using

TABLE I. Hydrostatic-pressure-induced shifts in the Curie-Weiss temperature T_0 obtained from conductivity data and dielectric-constant data. Also tabulated are T^* values to be used in Eq. (6).

Material	$-\partial T_0/\partial p$ ($^{\circ}\text{C}/\text{kbar}$)		T^* ($^{\circ}\text{K}$)
	σ	ϵ	
KTaO ₃	5.1 ± 0.5	5.1 ± 0.5	140 ± 25
SrTiO ₃	3.8 ± 0.5	3.8 ± 0.5	77 ± 18
KTa _{0.98} Nb _{0.02} O ₃	5.9 ± 0.5	5.1 ± 0.5	70 ± 22
BaTiO ₃ ^a	...	5.2 ± 0.7	85 ± 15

^a The ϵ value of $-\partial T_0/\partial p$ is taken from Ref. 7.

standard dc techniques on van der Pauw sample shapes prepared as described above. A heated sample chamber allowed measurements to be made to approximately 1000 $^{\circ}\text{K}$. For temperatures below room temperature a thermoelectric cooling unit was used. Conventional current and field reversal procedures were used to minimize the influence of extraneous potentials. In Fig. 3 we show Hall-mobility data for six perovskite crystals taken above their Curie temperatures. The SrTiO₃ values are taken from Ref. 1. It is clear from Fig. 3 that there exists a general trend of decreasing temperature dependence with increasing values of T_0 . We show below that this result is consistent with Eq. (6). Before doing this, however, it is important to separate out mobility μ and free-carrier-concentration n contributions to the conductivity given by Eq. (6). This presents no difficulty in KTaO₃ and SrTiO₃ since donors in these materials are very shallow^{1,8} and are generally fully ionized to temperatures as low as 4.2 $^{\circ}\text{K}$. As a result, we do not expect a pressure dependence of n . A similar conclusion holds for BaTiO₃ in which a

⁸ S. H. Wemple, Phys. Rev. **137**, A1575 (1965).

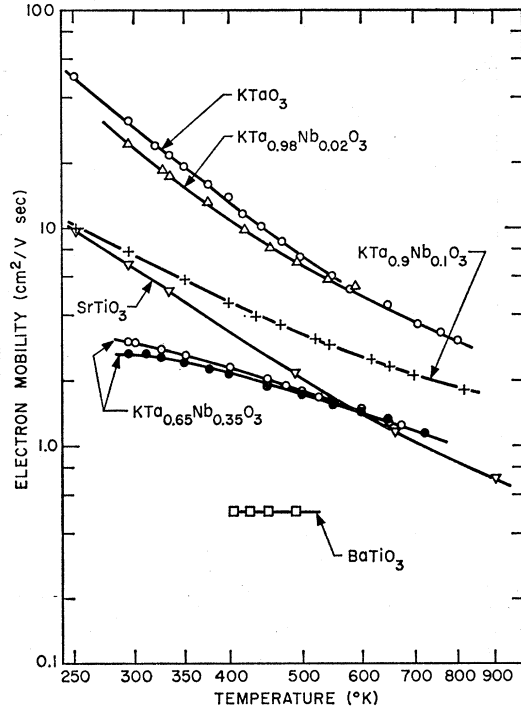


FIG. 3. Electron Hall-mobility temperature variation in the range $T > T_0$ in six perovskite-oxide ferroelectrics.

shallow donor is completely ionized, and a deep donor is essentially filled over the temperature range of the measurements.⁹ In the case of KTa_{0.65}Nb_{0.35}O₃, on the other hand, we have a deep donor situation¹⁰ with the Fermi level falling between the conduction band and the deep donor located 0.3 eV below the band edge. Even for this case we believe that the observed pressure dependences which lead to Eq. (6) are due to a pressure dependence of μ rather than n . This conclusion is based on the following arguments:

(i) The conductivity increases *linearly* with hydrostatic pressure by a factor of nearly 3 in contradiction to the *exponential* dependence expected, if changes in n due to donor level shifts were producing the conductivity increase.

(ii) An increase in n by a factor of approximately 3 would require that the donor binding energy decrease by approximately $2kT/e = 0.05$ eV, where k is Boltzmann's constant and e is the electronic charge. This 17% decrease would be excessively large, considering that the maximum lattice strain at even the highest pressures is less than 1%.

(iii) The agreement between the reciprocal pressure derivatives for both σ and ϵ data (see Table I) would be merely a coincidence if a different mechanism for the conductivity pressure dependence were operative in KTa_{0.65}Nb_{0.35}O₃.

⁹ C. N. Berglund and W. S. Baer, Phys. Rev. **157**, 358 (1967).

¹⁰ M. DiDomenico, Jr., and S. H. Wemple, Phys. Rev. **166**, 565 (1968).

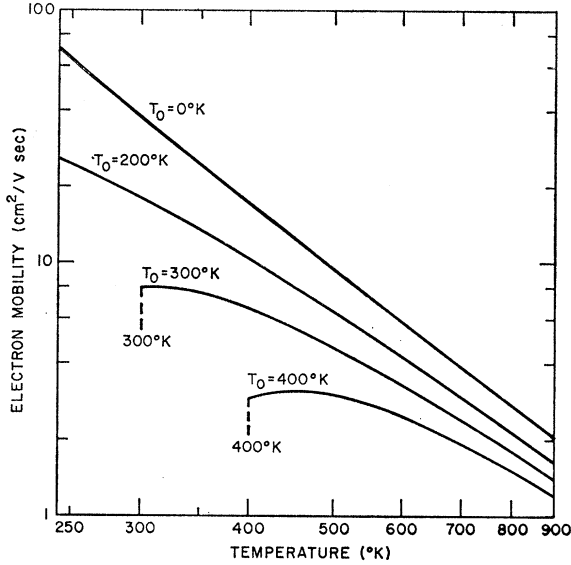


FIG. 4. Plot of the empirically derived relation $\mu \propto T^{-3.5} (T - T_0 + T^*)$ with $T^* = 100^\circ\text{K}$ (see Table I) for various values of T_0 . The mobility scale has been adjusted arbitrarily so that $\mu = 8 \text{ cm}^2/\text{V sec}$ when $T_0 = 300^\circ\text{K}$.

Based on the above arguments, we conclude that Eq. (6) can be rewritten

$$\mu = f(T)(T - T_0 + T^*), \quad T > T_0 \quad (7)$$

where $f(T)$ is related to $g(T)$ by a constant factor. An approximate empirical expression for the temperature-dependent prefactor $f(T)$ can be extracted from the curves shown in Fig. 3. As a final empirical result for temperatures below approximately 600°K , we find

$$\mu \propto T^{-3.5}(T - T_0 + T^*), \quad T > T_0. \quad (8)$$

In order to illustrate the influence of T_0 on the mobility temperature dependence described by Eq. (8) we have plotted μ versus T for $T^* = 100^\circ\text{K}$ and various values of T_0 in Fig. 4. The mobility scale has been selected arbitrarily to facilitate comparison with the data of Fig. 3. We note by comparing Figs. 3 and 4 that the qualitative features of the observed mobility temperature dependences (in the range $T < 800^\circ\text{K}$) are well described by Eq. (8); i.e., (i) the temperature dependence becomes weaker as T_0 increases, (ii) for $T_0 \approx 0^\circ\text{K}$ (KTaO_3), we find that $\mu \propto T^{-3}$, and (iii) for $T_0 \approx 400^\circ\text{K}$ (BaTiO_3), we find that μ is very weakly temperature dependent and is approximately constant for $400 < T < 600^\circ\text{K}$. A more detailed comparison between Figs. 3 and 4 cannot be made since different values of T_0 occur in different crystals. This leads to mobility scales which will not be exactly the same for all crystals since, for example, the electron effective masses are not necessarily identical. To overcome this difficulty we have measured the conductivity temperature dependences in $\text{KTa}_{0.65}\text{Nb}_{0.35}\text{O}_3$ and KTaO_3 at elevated pressures. We assume, for reasons given previously,

that the carrier-concentration temperature dependence is not affected by hydrostatic pressure, so that the only effect of pressure is to decrease T_0 in Eq. (8). We therefore expect a stronger temperature dependence at high pressures than at zero pressure (see Fig. 4). We also expect a more pronounced effect of pressure on the temperature dependence for high values of T_0 than for low values of T_0 . These expectations are borne out experimentally as shown in Fig. 5, where we have plotted $\ln \mu$ versus $\ln T$ for KTaO_3 ($T_0 = 4^\circ\text{K}$) and $\text{KTa}_{0.65}\text{Nb}_{0.35}\text{O}_3$ ($T_0 = 287^\circ\text{K}$) at two values of hydrostatic pressure. A substantial increase in the mobility temperature dependence with pressure is evident for $\text{KTa}_{0.65}\text{Nb}_{0.35}\text{O}_3$, whereas no significant change is observed for KTaO_3 . To calculate the mobility temperature dependence in $\text{KTa}_{0.65}\text{Nb}_{0.35}\text{O}_3$ at $p = 18.4 \text{ kbar}$ from the observed conductivity temperature dependence, we have made use of the zero-pressure carrier-concentration versus temperature data shown in Fig. 6. The indicated smoothed curve was then used to calculate the curves of Fig. 5.

In Fig. 7 we compare quantitatively the measured mobility temperature dependences at $p = 0 \text{ kbar}$ and $p = 18.4 \text{ kbar}$ in $\text{KTa}_{0.65}\text{Nb}_{0.35}\text{O}_3$ with those predicted by Eq. (8). Taking $T_0 = 287^\circ\text{K}$, $T^* = 70^\circ\text{K}$, and $\partial T_0/\partial p = -5.5^\circ\text{K/kbar}$ from Table I and fixing the zero-pressure mobility at room temperature to be $2.7 \text{ cm}^2/\text{V sec}$, we obtain the solid curves shown in Fig. 7. We conclude from the agreement between experiment and theory shown in Fig. 7 that the large change in mobility temperature dependence produced by hydrostatic pressure in $\text{KTa}_{0.65}\text{Nb}_{0.35}\text{O}_3$ is quantitatively predicted by Eq. (8). The insensitivity of the mobility temperature dependence to hydrostatic pressure in KTaO_3 is also quantitatively consistent with Eq. (8). To show this we

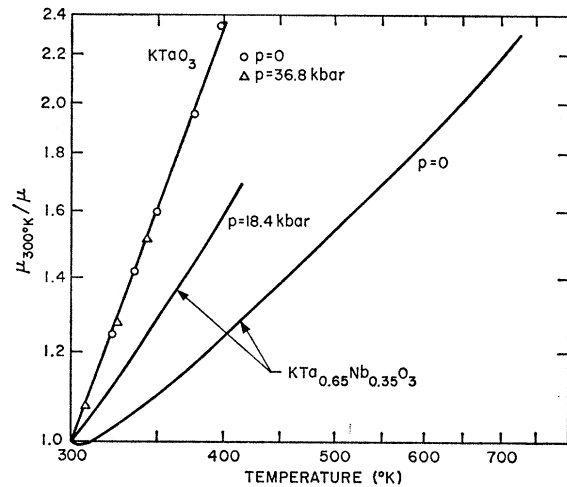


FIG. 5. Logarithmic plot of the temperature dependence of the Hall mobility in KTaO_3 and $\text{KTa}_{0.65}\text{Nb}_{0.35}\text{O}_3$ at two values of hydrostatic pressure, $\mu_{300^\circ\text{K}}$ refers to the mobility measured at $T = 300^\circ\text{K}$.

note, using Eq. (8), that

$$\frac{\partial}{\partial p} \left(\frac{\partial \ln \mu}{\partial \ln T} \right) = \frac{T \partial T_0 / \partial p}{(T - T_0 + T^*)^2}. \quad (9)$$

From Table I, taking $\partial T_0 / \partial p = -5.1^\circ\text{K}/\text{kbar}$, $T^* = 140^\circ\text{K}$, we obtain $(\partial/\partial p)(\partial \ln \mu / \partial \ln T) \approx -8 \times 10^{-3} \text{ kbar}^{-1}$ at $T = 300^\circ\text{K}$. The predicted increase in the quantity $\partial \ln \mu / \partial \ln T$ at $p = 36.8 \text{ kbar}$ is then approximately 0.3. The zero-pressure slope from Fig. 5 is 2.9 ± 0.1 in KTaO_3 , so that the negligible effect of pressure on the mobility temperature dependence is consistent with Eq. (8).

In summary, all of our experimental results on several perovskite materials at a variety of temperatures and pressures are consistent with a single empirical expression [Eq. (8)]. In Sec. III we show that this result is not consistent with existing electron scattering theories. We then propose in Sec. IV a new scattering mechanism which attributes electron scattering to wave packets of TO phonons associated with polarization fluctuations.

III. APPLICABILITY OF EXISTING THEORIES

Electron transport in wide-band-gap semiconductors has generally been interpreted using either a localized hopping model or a Bloch band model, depending on the degree of interaction between atoms in the crystal. Previously it had been thought that the interaction between d orbitals in d -band semiconductors is too weak to form broad Bloch-like conduction bands. Consequently, the localized electron hopping model has often been invoked¹¹ to explain transport phenomena in these materials. There is considerable experimental

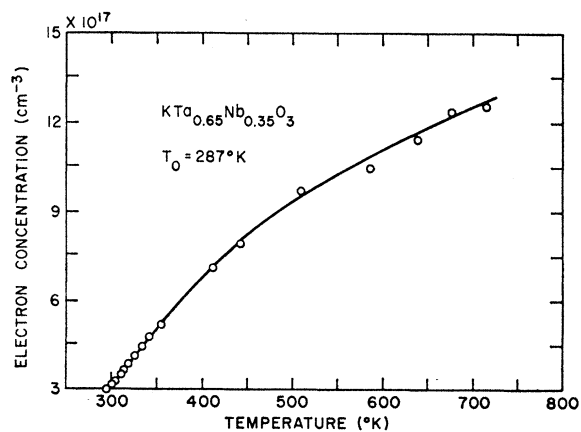


FIG. 6. Variation of the zero-pressure electron concentration with temperature in $\text{KTa}_{0.65}\text{Nb}_{0.35}\text{O}_3$.

¹¹ See, for example, F. J. Morin, in *Semiconductors*, edited by N. B. Hannay (Reinhold Publishing Corporation, New York, 1959).

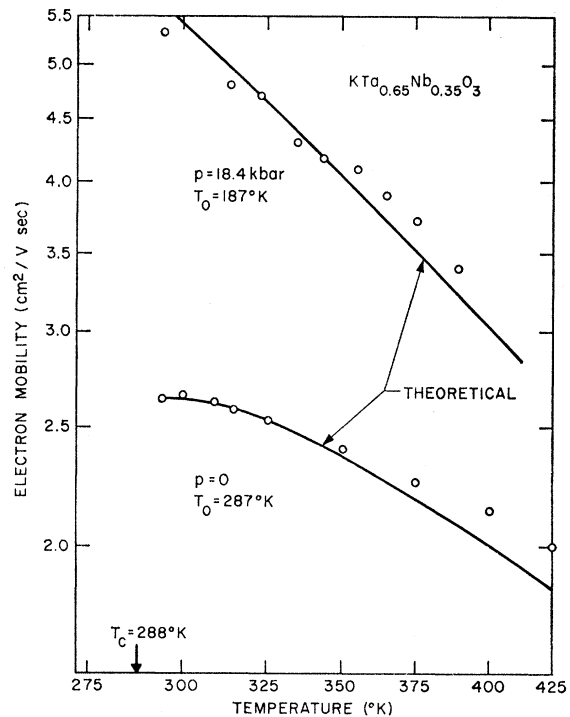


FIG. 7. Quantitative comparison of the experimental mobility (open circles) and the "theoretical" predictions (solid curves) at two values of hydrostatic pressure (0 and 18.4 kbar) in $\text{KTa}_{0.65}\text{Nb}_{0.35}\text{O}_3$. The theoretical curves obtained from Eq. (8) have been fitted to the experimental data at $p = 0$ and $T = 289^\circ\text{K}$. $T_c = 288^\circ\text{K}$ refers to the paraelectric-ferroelectric transition temperature.

evidence,^{10,12,13} however, that the d -band perovskite oxides containing $\text{Ti}(3d)$, $\text{Nb}(4d)$, or $\text{Ta}(5d)$ ions have broad conduction bands. Calculations of the energy-band structure of SrTiO_3 have been made by Kahn and Leyendecker,¹⁴ using the tight-binding method. Their results, which should extend to other perovskite oxides, indicate that the lowest conduction band is derived primarily from the titanium $d\epsilon$ d orbitals with an admixture of oxygen $2p$ orbitals. These authors also proposed that in cubic SrTiO_3 the overlap of the $d\epsilon$ orbitals across the full unit cell causes the conduction-band minima to fall at the Brillouin-zone (BZ) boundary along the three equivalent $\langle 100 \rangle$ directions. This many-valley model is consistent with a large number of experimental observations in several perovskite oxides.^{9,10,13,15-19}

¹² M. Cardona, *Phys. Rev.* **140**, A651 (1965).

¹³ C. N. Berglund and H. J. Braun, *Phys. Rev.* **164**, 790 (1967).

¹⁴ A. H. Kahn and A. J. Leyendecker, *Phys. Rev.* **135**, A1321 (1964).

¹⁵ H. P. R. Frederikse, W. R. Hosler, and W. R. Thurber, *Phys. Rev.* **143**, 648 (1966).

¹⁶ I. Camlibel (unpublished).

¹⁷ H. P. R. Frederikse, W. R. Hosler, W. R. Thurber, J. Babiskin, and P. G. Siebenmann, *Phys. Rev.* **158**, 775 (1967).

¹⁸ See, for example, C. S. Koonce, M. L. Cohen, J. F. Schooley, W. R. Hosler, and E. R. Pfeiffer, *Phys. Rev.* **163**, 380 (1967).

¹⁹ W. S. Baer, *J. Phys. Chem. Solids* **28**, 677 (1967).

In order to justify further our use of a Bloch band picture in the d -band perovskite oxides, it is of interest to examine electron effective masses using the many-valley model. We would expect a general trend of smaller effective masses (and higher mobilities) in order of increasing principal quantum number of the d band, as a result of the increasing extent of the radial wave functions in the sequence Ti($3d$), Nb($4d$), and Ta($5d$). Thus, the lowest effective masses are expected in tantalates and the highest in titanates. Based on a tight-binding interpolation between symmetry points in the BZ, it is easy to show that the appropriate bandwidths in transverse (m_t^*) and longitudinal (m_l^*) mass directions, viz., $\Delta\mathcal{E}_B^t$ and $\Delta\mathcal{E}_B^l$, are given by

$$\Delta\mathcal{E}_B^t \approx m_0/m_t^* \text{ eV} \quad \text{and} \quad \Delta\mathcal{E}_B^l \approx m_0/m_l^* \text{ eV}, \quad (10)$$

where m_0 is the free-electron mass. In Table II we summarize the effective-mass values and list the approximate conduction bandwidths obtained from Eq. (10). We conclude from these results that $\Delta\mathcal{E}_B \gg kT/e$, so that in the perovskite oxides the interaction between d orbitals is strong enough to give wide Bloch-like conduction bands.

The strongly polar nature of the perovskite oxides, as evidenced by their large static dielectric constants, has led several authors to conclude that the dominant electron-phonon interaction, at least in SrTiO₃, involves scattering of polarons by LO phonons. This conclusion is based on the observed mobility temperature dependence in SrTiO₃. Tufte and Chapman²⁰ fit their results to the expression $\mu = 0.83 (e^{\Theta/T} - 1) \text{ cm}^2/\text{V sec}$, where $\Theta = 600^\circ\text{K}$, while Frederikse and Hosler¹ make use of the known LO phonon energies and bare effective masses to calculate the mobility temperature dependence predicted by the Low-Pines² (LP) theory. The latter authors then conclude, based on the fair agreement between theory and experiment, that the polaron-LO-phonon interaction is dominant in SrTiO₃, at least for temperatures above 300°K.

Several theories have been proposed²¹ which describe the polaron-LO-phonon interaction in terms of a coupling parameter α . This quantity is physically approximately twice the number of phonons which "dress" the bare electron. For a material having a single optical branch the coupling parameter α is given by

$$\alpha = (m^*/m_0)^{1/2} (13.6/E_{\text{LO}})^{1/2} (1/\epsilon_\infty - 1/\epsilon), \quad (11)$$

TABLE II. Effective masses and estimated conduction bandwidths in several perovskite-oxide ferroelectrics.

Material	m_t^*/m_0	m_l^*/m_0	$\Delta\mathcal{E}_B^t$ (eV)	$\Delta\mathcal{E}_B^l$ (eV)
KTaO ₃	0.4	1.2	2.5	0.8
SrTiO ₃	1.5	6.0	0.7	0.17
BaTiO ₃	1.5	7.5	0.7	0.13

²⁰ O. N. Tufte and P. W. Chapman, Phys. Rev. **155**, 796 (1967).

²¹ See, for example, T. D. Schultz [Phys. Rev. **116**, 526 (1959)] for a review of these theories.

where m^* is the bare effective mass, E_{LO} is the LO phonon energy in eV, ϵ_∞ is the optical frequency dielectric constant, and ϵ is the static dielectric constant. The situation is complicated somewhat in the perovskite oxides (O_h symmetry in their paraelectric phase) by the fact that these materials have three LO-phonon modes. In all the materials under consideration the LO phonons have zone-center energies of approximately²² 0.1, 0.06, and 0.02 eV. Equation (11) should apply for the 0.1-eV phonon, since it is the LO counterpart of the strong, low-frequency soft TO mode which is the major contributor to ϵ . Substituting $\epsilon_\infty \approx 5$, $\epsilon > 100$, and $E_{\text{LO}} = 0.1$ eV into Eq. (11) yields $\alpha_1 \approx 2(m^*/m_0)^{1/2}$. The corresponding relation, as given by Eagles,²³ for the LO phonon near 0.06 eV is $\alpha_2 \approx 0.5(m^*/m_0)^{1/2}$. Coupling to the third LO phonon at 0.02 eV is extremely weak and can be neglected. Taking m^* to be approximately equal to the conductivity mass [$m_c^* = 3(2/m_t^* + 1/m_l^*)^{-1}$], we find that $\alpha_1(\text{SrTiO}_3) \approx 2.8$, $\alpha_2(\text{SrTiO}_3) \approx 0.7$, $\alpha_1(\text{KTaO}_3) \approx 1.4$, and $\alpha_2(\text{KTaO}_3) \approx 0.35$. Polaron scattering theories which are applicable to this intermediate coupling range have been given by LP and by Feynman *et al.*²⁴ Schultz²¹ has given a detailed comparison of several existing polaron theories and emphasizes that these theories assume that the time between scattering events is sufficiently long to permit the electron energy to be sharp in comparison to kT , i.e., $\Delta\mathcal{E}_r \ll kT/e$, where $\Delta\mathcal{E}_r \sim \hbar/\tau_e$ is a lifetime energy broadening (τ_e is the electron relaxation time and \hbar is Planck's constant). Using the relation $\tau_e \approx m_c^* \mu/e$, we find at room temperature that $\tau_e \approx 10^{-14}$ sec in KTaO₃ ($\mu = 31 \text{ cm}^2/\text{V sec}$) and SrTiO₃ ($\mu = 6 \text{ cm}^2/\text{V sec}$), and that $\tau_e \approx 10^{-15}$ sec in BaTiO₃ ($\mu \approx 0.5 \text{ cm}^2/\text{V sec}$).⁵ The corresponding values of $\Delta\mathcal{E}_r$ are ≈ 0.1 and ≈ 1 eV, respectively. We conclude that $\Delta\mathcal{E}_r \gg kT/e$ (throughout the lattice scattering range $T \gtrsim 100^\circ\text{K}$), thereby precluding the use of time-dependent perturbation theory and casting doubt on the usefulness of existing polaron theories.

Frederikse and Hosler,¹ in their analysis of mobility data in SrTiO₃, have nonetheless used the LP expression for the polaron relaxation time $\tau_p = \mu m^*/e$ given by

$$\tau_p = \frac{f(\alpha)}{2\alpha(1 + \frac{1}{6}\alpha)^3} \frac{e^{\hbar\omega_{\text{LO}}/kT}}{\omega_{\text{LO}}}, \quad (12)$$

in which $\hbar\omega_{\text{LO}}$ is the LO phonon energy and $f(\alpha)$ is a slowly varying function of α given by LP. Equation (12) further requires that $\hbar\omega_{\text{LO}} \gg kT$, i.e., only the slow polaron is considered. In order to use Eq. (12) in the temperature range $\hbar\omega_{\text{LO}} \lesssim kT$, Frederikse and Hosler replace $e^{\hbar\omega_{\text{LO}}/kT}$ by the Bose factor $e^{\hbar\omega_{\text{LO}}/kT} - 1$. This procedure is questionable, since the α -dependent co-

²² See A. S. Barker, Jr., in *Ferroelectricity*, edited by E. F. Weller (Elsevier Publishing Co., Inc., Amsterdam, 1967), p. 213.

²³ D. M. Eagles, J. Phys. Chem. Solids **26**, 672 (1965).

²⁴ R. P. Feynman, R. W. Hellworth, C. K. Iddings, and P. M. Platzman, Phys. Rev. **126**, 1004 (1962).

efficient in Eq. (12) was derived in the low-temperature limit. Furthermore, these authors have evaluated without theoretical justification a combined relaxation time for scattering by the 0.1- and 0.06-eV phonons by adding reciprocally the separate relaxation times calculated from Eq. (12). The above objections raise the possibility that the fair agreement noted between the calculated (using the LP theory) and the measured mobilities in SrTiO_3 may not warrant a firm conclusion as to the nature of the dominant scattering mechanism in this material. The agreement is in fact rather poor at low temperatures (below 300°K), where the LP theory is expected to be most applicable. If, indeed, the rough magnitude agreement is fortuitous, what conclusions can be drawn from the approximately exponential dependence of mobility on reciprocal temperature in SrTiO_3 observed by Tufte and Chapman,²⁰ by Frederikse and Hosler,¹ and by Parke and Yahia?²⁵ These data yield activation energies near room temperature in the vicinity of 0.06 eV, a value close to the energy of an LO phonon in SrTiO_3 . We note first that exponential and power-law temperature dependences are difficult to distinguish over a limited temperature range. This is made clear in Fig. 8, where we have plotted mobility on a logarithmic scale versus $10^3/T$ for KTaO_3 , SrTiO_3 , and $\text{KTa}_{0.65}\text{Nb}_{0.35}\text{O}_3$. The solid curves are given by the relation $\mu \propto T^{-n}$, where n has the values indicated in the figure. The dashed curves are given by $e^{\hbar\omega_{\text{LO}}/kT}$, where $\hbar\omega_{\text{LO}} = 0.1$ eV corresponding to the highest LO phonon energy. Thus, values of n between 2 and 3 correspond to apparent activation energies not very different from observed LO phonon energies in the perovskite oxides. A second observation is that $\text{KTa}_{0.65}\text{Nb}_{0.35}\text{O}_3$ has a much weaker mobility temperature dependence than the other two materials. An even weaker dependence is observed in BaTiO_3 (see Fig. 4). Since all of these perovskite oxides have very nearly the same LO phonon energies, we conclude that (i) the scattering mechanisms differ from material to material, or (ii) the same scattering mechanism applies, but it does not involve LO phonons. The experimental results presented in Sec. II strongly support the latter viewpoint. For example, Eq. (8) is not consistent with the polaron-LO-phonon interaction. In the polaron model the static dielectric constant ϵ enters into the mobility through the coupling parameter α [Eq. (11)]. Since $\epsilon \gg \epsilon_\infty$, the dielectric constant dependence of this interaction is extremely weak. In addition, the LO phonon energies do not depend strongly on hydrostatic pressure. As a result, the polaron mobility [Eq. (12)] is not expected to vary linearly with hydrostatic pressure.

Another model, the hopping small polaron, has been proposed²⁶ to explain electron transport in low-mobility polar materials. For the small polaron model to hold,

²⁵ D. Parker and J. Yahia, *Phys. Rev.* **169**, 605 (1968).

²⁶ See, for example, H. G. Reik, *Solid State Commun.* **1**, 68 (1963).

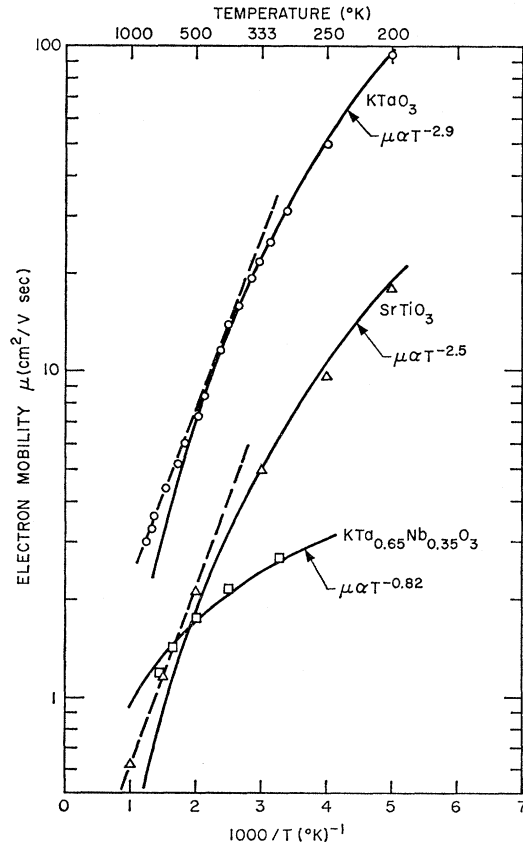


Fig. 8. Electron Hall mobility versus $10^3/T$ in KTaO_3 , SrTiO_3 , and $\text{KTa}_{0.65}\text{Nb}_{0.35}\text{O}_3$. The solid curves are power-law fits to the data. The dashed curves correspond to exponential dependences $e^{\Theta/T}$, with $\Theta \approx 1200^\circ\text{K}$, i.e., an activation energy of 0.1 eV.

narrow bands are required (i.e., $\Delta\mathcal{E}_B \lesssim kT/e$), so that the electron can be self-trapped by the lattice distortions produced by the Coulomb field of the electron. Electron transport then involves thermally activated hopping between nearly localized sites. As we have pointed out, there is considerable evidence that $\Delta\mathcal{E}_B \gg kT/e$ in the perovskite oxides leading to a wide-band rather than to a narrow-band picture. Further arguments against the small polaron model are provided by mobility and optical-absorption data. According to the small polaron description, the mobility should increase with increasing temperature, whereas experimentally it is observed to decrease. The small polaron model also predicts a peak in the optical absorption in the near-infrared spectral region. In analyzing the optical absorption spectrum of semiconducting BaTiO_3 , Gerthsen *et al.*²⁷ interpret the broad infrared absorption peak near 0.6 eV in terms of a small polaron interaction. Berglund and Braun¹³ and DiDomenico and Wemple¹⁰ show, however, that the 0.6-eV absorption peak occurring in semiconducting crystals of BaTiO_3 and $\text{KTa}_{0.65}\text{Nb}_{0.35}\text{O}_3$ is due to deep donor photoionization into a broad conduction band.

²⁷ P. Gerthsen, R. Groth, K. H. Hardtl, D. Heise, and H. G. Reik, *Solid State Commun.* **3**, 165 (1965).

IV. CRITICAL-POINT FLUCTUATION MODEL OF ELECTRON SCATTERING

In this section we propose a new electron-phonon interaction which is consistent with the experimental results presented in Sec. II. As a starting point, we observe that an experimental relationship exists between the electron mobility and the static dielectric constant [cf. Eq. (2)]. Since the static dielectric constant is almost totally determined by the strength of the lowest-frequency TO lattice mode, it would appear, as previously proposed,⁹ that the electron-TO-phonon interaction predominates in these materials. Normally such an interaction is considered to be either nonexistent or exceedingly weak, since there are no macroscopic electric fields associated with TO phonons as there are with LO phonons. The perovskite oxides are unusual, however, in that the amplitude of the low-frequency (soft) TO phonon is very large. This can be seen by noting that the thermally stimulated soft-mode amplitude is proportional to the lattice-polarization fluctuation δP . It is a well-known thermodynamic result that the mean-square polarization fluctuation amplitude $\langle \delta P^2 \rangle$ is given by²⁸

$$\langle \delta P^2 \rangle = kT\epsilon/V, \quad (13)$$

where V is a characteristic volume which we will take to be the volume of a polarization fluctuation cluster. According to Eq. (13), the mean-square TO phonon amplitude is directly proportional to ϵ and hence is expected to be unusually large in the paraelectric phase of the ferroelectric perovskite oxides. In Eq. (13), δP can be regarded as the average polarization of the volume V , provided that V is large enough so that classical macroscopic models apply. Physically, the cluster volume V is determined by the range over which the polarization amplitude remains spatially correlated. As discussed below, the correlation length is expected to be at least several lattice constants long, making the volume V large enough to ensure the validity of Eq. (13). We emphasize at this point that lattice-polarization fluctuations as described by Eq. (13) have been observed directly in perovskite ferroelectrics in Raman scattering experiments.²⁹

In order to describe the electron coupling to the thermally induced polarization fluctuations, we use an approach conceptually analogous to the deformation-potential methods³⁰ that have been applied, for example, to acoustic-mode scattering in semiconductors. Shifts in the conduction-band edge can be written phenomenologically in the form

$$\Delta \mathcal{E}_c = \mathfrak{D}\Delta + \beta\delta P^2 + \dots, \quad (14)$$

where $\Delta \mathcal{E}_c$ is the band-edge shift, Δ is the local dilatation amplitude, and δP is the polarization fluctuation amplitude. The quantities \mathfrak{D} and β are, respectively, the deformation-potential and the polarization-potential parameters. Terms linear in δP are omitted since the crystals under consideration possess a center of inversion symmetry for $T > T_0$. In writing Eq. (14) we have omitted the tensor properties of the various quantities for clarity. To compare the size of the deformation-potential energy shift $\mathfrak{D}\Delta$ with the polarization-potential energy shift $\beta\delta P^2$, we assume that \mathfrak{D} and β have the typical values $\mathfrak{D} \sim 10$ eV and $\beta \approx 2$ eV m⁴/C² (e.g., see Ref. 10). Using statistically averaged values of Δ and δP^2 , it can be shown that in the temperature range of interest $\beta\delta P^2 > \mathfrak{D}\Delta$, leading us to conclude that scattering by acoustic modes is negligible. In the usual deformation-potential theory of scattering the electron-phonon interaction is proportional to $\mathfrak{D}\Delta$ and is *linear* in the local lattice distortion. However, in the perovskite ferroelectrics the proposed electron-phonon interaction in the paraelectric phase ($T > T_0$) is *quadratic* in the soft-TO-phonon lattice distortion. It is worth noting that the polarization-potential interaction $\Delta \mathcal{E} = \beta\delta P^2$ has been used previously with considerable success to compute absolute Raman scattering efficiencies³¹ and electro-optic and nonlinear optic effects³² in perovskite ferroelectrics.

The polarization fluctuation clusters can be related to the soft-TO-phonon dispersion curve. In Fig. 9 we

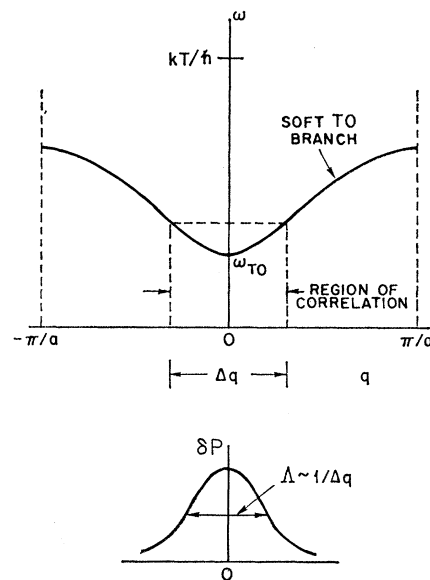


Fig. 9. Real-space and q -space representations of soft-TO-phonon wave packet. Δq is a phonon coupling range. $\Lambda \sim 1/\Delta q$ is the corresponding real-space width of the phonon wave packet or polarization fluctuation cluster.

²⁸ See, for example, *Fluctuation Phenomena in Solids*, edited by R. E. Burgess (Academic Press Inc., New York, 1965).

²⁹ M. DiDomenico, Jr., S. P. S. Porto, and S. H. Wemple, *Phys. Rev. Letters* **19**, 855 (1967); M. DiDomenico, Jr., S. H. Wemple, S. P. S. Porto, and R. P. Bauman, *Phys. Rev.* **174**, 522 (1968).

³⁰ See, for example, W. Shockley, *Electrons and Holes in Semiconductors* (D. Van Nostrand, Inc., New York, 1950).

³¹ S. H. Wemple and M. DiDomenico, Jr., in *Light Scattering in Solids*, edited by G. B. Wright (Springer-Verlag, Berlin, 1969), Paper A-5.

³² M. DiDomenico, Jr., and S. H. Wemple, *Appl. Phys. Letters* **12**, 352 (1968); *J. Appl. Phys.* **40**, 720 (1969).

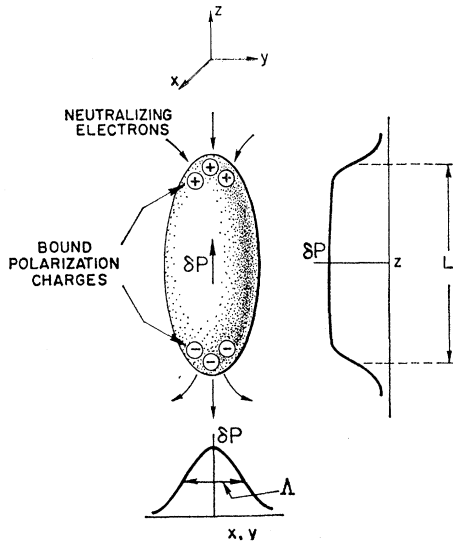


FIG. 10. Schematic representation of a polarization fluctuation cluster. Shown are the bound polarization charges $\nabla \cdot \delta \mathbf{P}$ terminating a cluster and the space charge screening free electrons. The lengths Λ and L are temperature-dependent correlation lengths.

indicate the expected spatial variation of the polarization fluctuation amplitude within a cluster and the corresponding region of correlation in q space. The TO phonons contained in the range $\Delta q \sim 1/\Lambda$, where Λ is the real-space spatial correlation length, form a TO-phonon wave packet. To see how this comes about we note that the spatial correlation function is given by³³

$$\langle \delta P(0) \delta P^*(r) \rangle \propto \sum_q \langle |a_q|^2 \rangle e^{iqr}, \quad (15)$$

where a_q is the amplitude of a TO mode with wave number q (the asterisk denotes the complex conjugate). Since the soft-TO-phonon branch can be treated classically in the perovskite ferroelectrics (see Fig. 9), we have $\langle |a_q|^2 \rangle \propto kT/\omega_q^2$. Therefore the correlation function decreases as q increases, and we find that over the region of correlation $\Delta q \sim 1/\Lambda$ the polarization fluctuation maintains a finite amplitude. In three dimensions we view each fluctuating cluster at a fixed time as a needle whose long dimension coincides with the δP axis as shown in Fig. 10. The needlelike shape arises from the fact that $\nabla \cdot \delta \mathbf{P} = 0$, so that spatial variations of δP along the direction of δP are absent. This same conclusion can be reached by taking into account in Eq. (15) the anisotropy in the TO-phonon dispersion curves along different principal axes in q space. Note that the δP axis coincides with the direction of maximum dipolar coupling. Each cluster, of course, must end, and, as indicated in Fig. 10, there is a depolarizing field associated with $\nabla \cdot \delta \mathbf{P}$ near the end of each needle. This field is screened by the free charges which are present. Since, as pointed out earlier, the electron relaxation time is of the order 10^{-14} sec, and since the period of the fluctuation motion, which is connected

with the soft-TO-phonon lifetime, is of the order 10^{-12} sec, almost complete screening can take place.

The spatial correlation lengths L and Λ shown in Fig. 10 can be described qualitatively in terms of the ferroelectric properties of the perovskite crystal structure. Along the direction of δP the correlation between values of δP in neighboring cells is a consequence of the same strong "bootstrap" mechanism which leads to ferroelectricity. Thus, the correlation length L along the δP axis should be long, resulting in the formation of long dipolar chains having a TO-phonon character. In directions normal to δP , however, the "forces" which tend to produce parallel alignment of dipoles are much weaker. Physically this comes about because an antiparallel alignment of free electric dipoles is energetically favorable in directions normal to the dipolar axis. However, the antiparallel arrangement introduces elastic strain energy between neighboring cells which is not present in the parallel arrangement. Consequently, a balance between dipolar and elastic forces determines the correlation length Λ . An estimate for the magnitude of Λ can be obtained from the theory of 180° antiparallel domain walls in ferroelectric BaTiO_3 .^{34,35} When elastic forces are taken into account these theories yield wall thickness of two to five lattice constants, i.e., 10–20 Å. We expect that Λ will not differ substantially from this estimate.

Based on the foregoing, we conclude that a three-dimensional array of needlelike quasistatic polarization fluctuation clusters comprises the "disturbed" lattice. In our model, electrons are scattered by these fluctuations via the polarization-potential interaction. Since the polarization potential relates δP to energy-band shifts according to Eq. (14), the electron can be viewed as traversing a three-dimensional, nonuniform distribution of band-edge energies. A complete analysis of the scattering problem must take into account the many-valleyed nature of the conduction band. Figure 11(a) shows schematically the constant energy surfaces appropriate to the perovskite oxides in the absence of a polarization fluctuation.¹⁴ In the presence of a polarization fluctuation δP the two valleys lying perpendicular to the δP axis are raised in energy, whereas the third valley remains relatively unaffected¹⁰ as indicated in Fig. 11(b). The polarization-potential-related interaction thus effectively couples to electrons in the valleys perpendicular to δP . We can introduce on physical grounds a scattering anisotropy for electrons in a particular valley. This comes about because longitudinal and transverse masses have their origin in quite different wave-function overlaps. The perovskite unit-cell structure and the regions of important p and d orbital overlap are shown schematically in Fig. 12. The $pd\pi$ interaction gives rise to the transverse mass, and the $dd\delta$ interaction (via the A -site cation) gives rise to the larger longitudinal mass. Optical-mode lattice vibrations will therefore

³⁴ W. Kinase, Progr. Theoret. Phys. (Kyoto) 13, 529 (1955).

³⁵ V. A. Zhirnov, Zh. Eksperim. i Teor. Fiz. 35, 1175 (1959) [English transl.: Soviet Phys.—JETP 35, 822 (1959)].

³³ We are grateful to C. Herring for pointing this out to us.

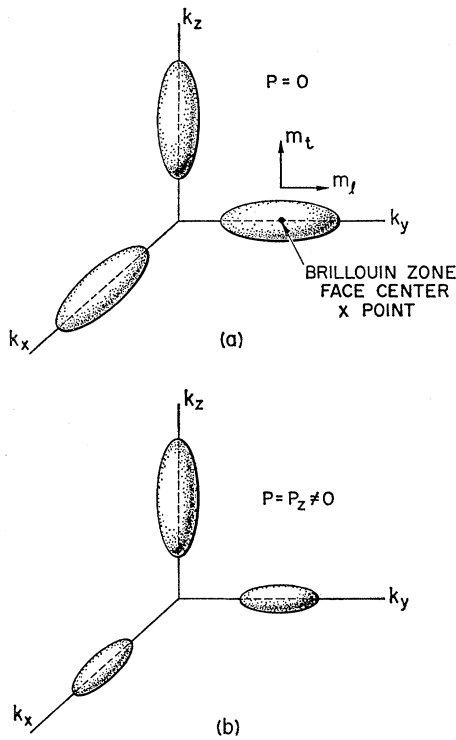


FIG. 11. Representation of the constant energy surfaces of the many-valleyed conduction-band structure appropriate to the perovskite oxides. (a) Band structure in the absence of crystal polarization; (b) structure in the presence of a z -directed polarization.

disturb electron transport differently in the low- and high-mass directions in k space. We suggest that the lowest-frequency TO phonon, which involves relative motion of the B cation against the oxygen-octahedron cage, will couple most strongly to transverse-mass electrons in valleys perpendicular to the polarization axis. Longitudinal-mass electrons will not be affected greatly by the TO-phonon vibrational motion. It is possible that LO phonons may couple to transverse-mass electrons in the parallel valley or to longitudinal-mass electrons in any valley.

Thus far we have described an electron-phonon interaction involving critical-point lattice-polarization fluctuations comprised of soft-TO-phonon wave packets. A detailed calculation of the scattering induced by this interaction is not available, although a simplified one-dimensional description has been given elsewhere.⁴ Since, as pointed out earlier, the uncertainty in electron energy greatly exceeds kT as a result of a very strong electron-phonon interaction, standard perturbation theory approaches to the scattering problem are not expected to apply. The empirical relation given by Eqs. (1) and (8) suggests that the net electron relaxation time τ_e varies as

$$\tau_e \propto c(T) \langle \delta P^2 \rangle^{-1} + \tau_0, \quad (16)$$

where $c(T)$ is a coupling factor characterizing the electron polarization-potential interaction and τ_0 repre-

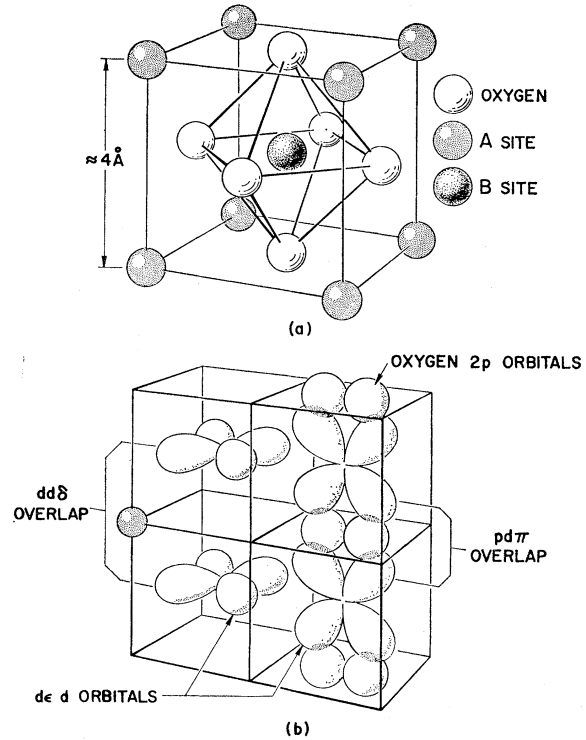


FIG. 12. (a) ABO_3 perovskite crystal structure showing BO_6 octahedron, where B denotes the transition-metal ion. (b) Orbital overlaps responsible for the transverse-electron effective mass ($pd\pi$ overlap) and longitudinal-electron effective mass ($dd\delta$ overlap).

sents a background lattice scattering contribution. Equation (16) gives the somewhat surprising result that relaxation times rather than relaxation rates add. This may be a consequence of the many-valley conduction-band structure and the way the polarization-potential interaction couples to the valleys (see Fig. 11). If we make the reasonable assumption that the background lattice scattering mechanism which gives rise to τ_0 is due to LO phonons, we find that $\tau_0 \propto e^{\Theta/T}$, where Θ is the Debye temperature of the highest-frequency LO mode. For $\Theta \approx 1200^\circ\text{K}$ ($\hbar\omega_{LO} = 0.1$ eV) and $100 < T < 1000^\circ\text{K}$, the factor $e^{\Theta/T}$ is almost indistinguishable from the power law $T^{-3.5}$. The importance of this observation is that it indicates a possible origin for the constant term in the experimental mobility expression given by Eq. (8). Extending the above line of reasoning further, we may conclude by comparing Eq. (16) with Eq. (8) and by making use of Eq. (13) that $c(T)V(T) \propto T^{-2.5}$, where $V(T)$ is the temperature-dependent polarization fluctuation cluster volume.

ACKNOWLEDGMENTS

It is a pleasure to thank C. Herring for helpful discussions and for critically reviewing the manuscript. We also thank A. Linz of MIT for the $BaTiO_3$ crystals, L. G. Van Uitert for the $KTaO_3$ and $KTa_{1-x}Nb_xO_3$ crystals, and I. Camlibel and R. G. Maines for their experimental assistance.